

# REACT: Real-time Efficiency and Accuracy Compromise for Tradeoffs in Scene Graph Generation

Maëlic Neau<sup>1,3,4 †</sup>  
maelic.neau@umu.se

Paulo E. Santos<sup>2,3</sup>  
paulo.santos@priorianalytica.com

Anne-Gwenn Bosser<sup>4</sup>  
boss@enib.fr

Cédric Buche<sup>5,6</sup>  
cedric.buche@cnrs.fr

Akihiro Sugimoto<sup>7</sup>  
sugimoto@nii.ac.jp

<sup>1</sup> Umeå University, Universitetstorget 4, Umeå, Sweden

<sup>2</sup> PrioriAnalytica, 74 Pirie St, Adelaide, Australia

<sup>3</sup> Flinders University, Sturt Rd, Bedford Park, Australia

<sup>4</sup> Bretagne INP - ENIB, 945 Av. du Technopôle, Plouzané, France

<sup>5</sup> CNRS IRL 2010 CROSSING, 11 Victoria Drive, Adelaide, Australia

<sup>6</sup> IMT Atlantique, 655 Av. du Technopôle, Plouzané, France

<sup>7</sup> National Institute of Informatics, 2-12 Hitotsubashi, Tokyo, Japan

## Abstract

Scene Graph Generation (SGG) is a task that encodes visual relationships between objects in images as graph structures. SGG shows significant promise as a foundational component for downstream tasks, such as reasoning for embodied agents. To enable real-time applications, SGG must address the trade-off between performance and inference speed. However, current methods tend to focus on one of the following: (1) improving relation prediction accuracy, (2) enhancing object detection accuracy, or (3) reducing latency, without aiming to balance all three objectives simultaneously. To address this limitation, we propose the Real-time Efficiency and Accuracy Compromise for Tradeoffs in Scene Graph Generation (REACT) architecture, which achieves the highest inference speed among existing SGG models, improving object detection accuracy without sacrificing relation prediction performance. Compared to state-of-the-art approaches, REACT is 2.7 times faster and improves object detection accuracy by 58%. Furthermore, our proposal significantly reduces model size, with an average of 5.5x fewer parameters. The code is available at <https://github.com/Maelic/SGG-Benchmark>.

# 1 Introduction

Scene Graph Generation (SGG) is the task of generating a structured graph representation from visual inputs. Given an image, visual regions corresponding to objects of interest are extracted, and relations between these objects are predicted in the form of  $\langle \text{subject}, \text{predicate}, \text{object} \rangle$  triplets. The set of these triplets forms a directed acyclic graph which can be interpreted as a structured representation of the scene. This task has garnered increasing attention recently thanks to its utility in various downstream applications, such as Visual Question Answering (VQA) [6, 8, 22], Image Captioning [29, 38, 42], or Reasoning of an embodied agent [9, 21, 23]. However, we observe a significant imbalance between the progress in the SGG task itself and its adoption in downstream tasks [9].

One of the reasons is the lack of low-cost approaches that could power applications with real-time constraints. Because SGG is a task that combines Object Detection (OD) and Relation Prediction (RelPred), a good trade-off between accuracy in these two parameters is also required. In this work, we explore the bottlenecks in SGG to find an optimal combination of OD accuracy, RelPred accuracy, and latency. SGG methods can be either Two-Stage (TS) or One-Stage (OS) approaches. The former uses a combination of an object detector and a relation predictor to model objects and relations in a sequence. The latter uses a single-stage pipeline to infer relations and object proposals directly from the image features. As a result, one-stage approaches are often more efficient for real-time processing [10]. However, they fall short in accuracy in the OD task [9, 19].

In this work, we investigate the bottlenecks of the two-stage architecture in terms of OD accuracy and latency. The structural dependencies between blocks of the architecture are reviewed as a Decoupled Two-Stage SGG (DTS-SGG), which allows maintaining the performance of the pre-trained detector, providing better control of the information flow (i.e., detected object proposals) between the two stages of the architecture. This approach reduces the overall latency, as the complexity of relation prediction increases exponentially with the number of input objects. To select an optimal amount of proposals at inference time, we define a new algorithm, the Dynamic Candidate Selection (DCS). DCS uses evaluation results to find the best trade-off between latency and accuracy at test time. Thanks to the DTS architecture, we can switch the dependency on a Faster-RCNN model for any real-time object detectors, such as one of the YOLO family (YOLOV8/9/10 [15, 36, 37]). Recent state-of-the-art SGG models such as PE-NET [24] use a combination of different feature sources, such as union pair features [25] or textual features of the subject and object classes [26]. This results in a significant amount of processing to gather and refine each type of feature altogether. By removing the dependency on sub-optimal features, we can reduce the parameter count of the model and lower the latency. By coupling this strategy to the DTS architecture, we propose a new model for

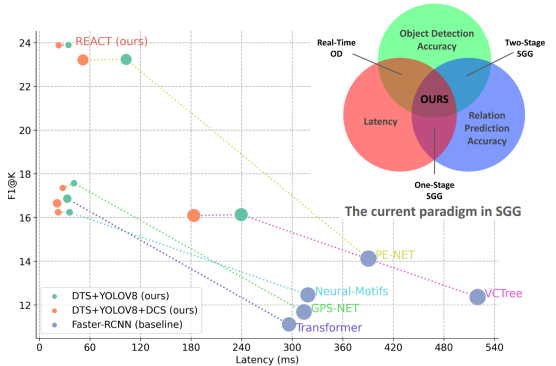


Figure 1: Performance comparison between our approach and previous work, in terms of performance (F1@K metric) and Latency (ms) on the PSG dataset [10]. Points are scaled by the number of parameters (smaller is better).

SGG, the Real-Time Efficiency and Accuracy Compromise for Tradeoffs in SGG (**REACT**). Thus, the main contributions of this work are: (i) a new architecture for SGG, the Decoupled Two-Stage (DTS); (ii) a new inference method, Dynamic Candidate Selection (DCS), which finds an optimal number of proposals to select for the relation prediction stage, to further improve latency without compromising accuracy; (iii) a new model, REACT, that extends previous work and our DTS architecture, reducing the latency while enhancing performance on standard metrics, see Figure 1.

## 2 Related Work

**Two-stage SGG approaches** typically use Faster-RCNN with a VGG-16 [69, 40] or ResNeXt-101 backbone for object detection and feature extraction, as seen in Neural-Motifs [43], VCTree [32], Transformer [63], GPS-Net [25], and PE-NET [44]. In these approaches, object classes probabilities given by Faster-RCNN are refined during relationship learning, via a dedicated classifier [25, 43] or by aggregating features from neighboring regions [40]. However, this design can hinder the performance of SGG models on the task of Object Detection. In our work, we choose to effectively *Decoupled* the Object Detector and Relationship Predictor by removing the dedicated classifier and keeping original class probabilities. In addition, Faster-RCNN’s large backbone limits real-time use. Recent work [10] proposed a real-time SGG method using contextual cues, relying on YOLOv5 [24] bounding boxes to learn correlations between box coordinates and predicates—excluding visual features. However, the method’s reliance on spatial features will neglect fine-grained relations such as the difference between *eating* or *drinking*. Another approach [13] uses a Relation-aware YOLO (RYOLO) to predict relation coordinates via new anchors, matched to nearby objects. Yet, lacking subject-object context leads to poor RelPred performance (3.1% mR@100) [43]. In contrast, we propose to use the features extracted by a YOLO model to generate representations for the subject and object nodes, making the first stage of the architecture more efficient without compromising performance on the second stage.

**One-stage SGG approaches** jointly learn object and relation representations. Sparse-RCNN [34] uses triplet queries to produce objects and relations, decoded via cascade-RCNN after CNN feature extraction. RelTr [9] and SGTR [20], built on DETR [10], generate sparse relation sets, unlike dense two-stage predictions. More recently, EGTR [11] builds upon Deformable-DETR for efficient object detection, paired with graph-based relation matching. RelTr and EGTR report lower latency than two-stage models like Motifs [43] and VCTree [32], though these comparisons often rely on Faster-RCNN. As highlighted in recent work [20], learning both the object and relation representations at the same time can make the performance of one-stage models in OD sub-optimal in comparison to two-stage approaches. We argue that replacing Faster-RCNN with YOLO in two-stage pipelines can achieve both lower latency than two-stage approaches and higher OD accuracy than one-stage approaches, as we shall see in this paper.

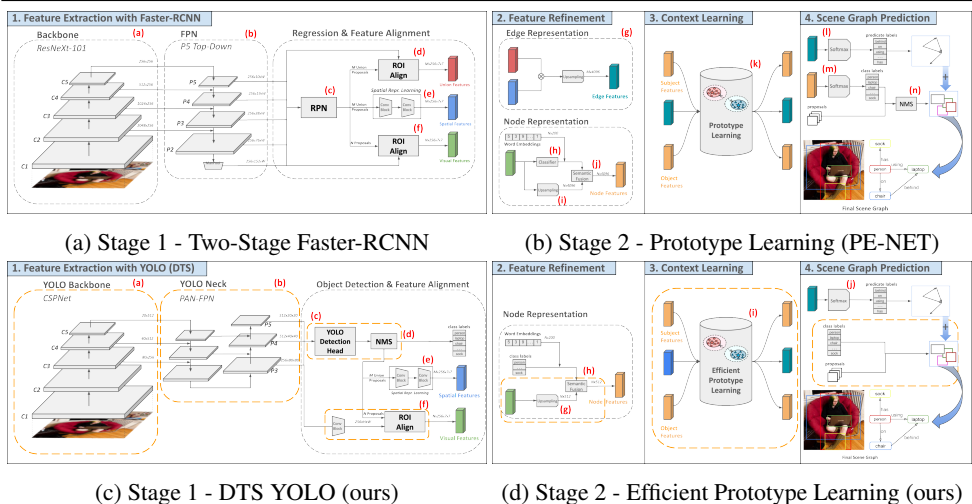


Figure 2: Top: the PE-NET architecture [44]. Bottom: our proposed REACT model with (left) Decoupled Two-Stage (DTS) + YOLO for efficient object detection and feature extraction ; (right) our proposed Efficient Prototype Learning model. [ - - - ] represent modified or added components,  $\otimes$  denotes element-wise concatenation.

### 3 Investigating Bottlenecks in SGG

Figure 2 (top row) is a representation of the PE-NET model [44]: a state-of-the-art two-stage SGG approach. The feature extraction (stage 1 Figure 2a) as well as the graph prediction (module 4, Figure 2b) are common to all two-stage architectures [6, 18, 25, 52, 53, 43]. In Stage 1, visual features are extracted by a ResNeXt-101 backbone (Figure 2a (a)), and a Feature Pyramid Network (FPN) [24] is used to refine the features at different scales (Figure 2a (b)). Then, a Region Proposal Network (RPN) [51] generates proposals (Figure 2a (c)) which are used to align three different types of features with corresponding image regions: union features, spatial features, and visual features (Figure 2a (d), (e), and (f)) using ROI Align [51]. Union and spatial features are aggregated for every possible pair of proposals and will serve as the initial edge representation to the relation prediction stage (Stage 2, Figure 2b). A classifier extracts the class labels of each proposal (Figure 2b (h)) and retrieves corresponding linguistic features from pre-trained text embeddings (GloVe [50]). Then, the visual features are combined with the textual features to form the node representation through semantic fusion (Figure 2b (i), (j)). Then, prototype learning takes place (Figure 2b (k)). Finally, object and predicate labels are decoded to form the final graph representation (Figure 2b (l), (m), and (n)). Below, we discuss the main bottlenecks of this architecture for Latency and Object Detection accuracy.

**Object Detection Accuracy.** The strategy employed in the two-stage SGG is to decode object labels twice during the relation prediction stage: one time for extracting text features (Figure 2b (h)) and one time to compute the final predictions (Figure 2b (m)). The predictions obtained from this last step depend on each model’s context learning strategy [25, 52, 53, 43]. This architecture design is (i) redundant as similar operations are performed twice, and (ii) can introduce significant differences in object detection accuracy in contrast to the original Faster-RCNN implementation. Table 1 draws a comparison of the

Backbone	Relation Head	mAP@50
Faster-RCNN	-	36.4
	Neural-Motifs [43]	35.9
	PE-NET [42]	35.4
	Transformer [63]	34.6
	VC-Tree [52]	32.6
	GPS-NET [25]	31.5

Table 1: OD accuracy for two-stage models compared to Faster-RCNN, PSG dataset [41].

performance of the Faster-RCNN model equipped with a ResNeXt-101 feature extractor on the PSG dataset with different relation prediction heads. We can observe that the performance in OD drops significantly, from 1 point wrt Motifs-TDE [43, 43] to almost 13 points in mAP@50 wrt GPS-NET [25] after the relation prediction stage. These results demonstrate a clear dependency between the two stages of the pipeline, which negatively impacts model performance on the object detection (OD) task. A second consideration given these results is the low performance of Faster-RCNN. Recent state-of-the-art detectors such as YOLOV8/9/10 may be more appropriate for the task. In contrast to Faster-RCNN, the YOLO architecture is not designed for Feature Extraction. This is the main reason why the Faster-RCNN architecture is still widely used for SGG.

**Proposal Candidate Selection.** In the TS architecture, Non-Maximum Suppression (NMS) for object proposals (Figure 2b (n)) is performed in stage 2. To alleviate the lack of NMS in stage 1, a fixed set of the top proposals is traditionally considered valid node candidates for stage 2. The idea here is that by sampling a large number of proposals per image, it is easier to find valid pairs and relations. However, this increases the computational complexity of the graph learning. Also, the number of top proposals to select (traditionally 80 or 100) is set arbitrarily. Recent work [18, 43, 43] computes the final ranking of relations with the following score formula:  $\theta_{rel} = \theta_{obj} * \theta_{pred} * \theta_{subj}$ , where  $\theta_{pred}$  is the confidence score of a predicate, given  $\langle subject, object \rangle$  pair as candidate; and,  $\theta_{obj}, \theta_{subj}$  are the respective confidence score of the object detector. This formulation assigns greater weight to the confidence scores of the subject and object compared to the predicate. As a result, many low-confidence proposals can be filtered out prior to the relation prediction stage with minimal impact on the model’s overall accuracy.

**Latency of the PE-NET model.** In PE-NET, node prototypes are formed using a combination of linguistic features and visual features (see Figure 2b (j)). Edge features are computed using the concatenation of the spatial and union features (see Figure 2b (g)). During prototype learning, prototype representations of the subject and object are combined and added to the edge features to form the relation prototype. Finally, a gate mechanism is employed to select relevant features from the multi-modal fusion. The use of both union and spatial features represents a considerable amount of overload for the model. In fact, another step of ROI Align is performed on the union of subject and object boxes (Figure 2a step (d)). However, visual information is already present in the object and subject features (see Figure 2a (f)), which will be fused with edge features during prototype learning. In addition, during edge and node feature refinement, all features are traditionally upsampled to a fixed size of 4096 (see Figure 2b (g) and Figure 2b (i)). However, larger feature sizes can significantly augment the latency of the model. Therefore, we aim to investigate the usage and size of each feature type to find an optimal trade-off between latency and performance.

## 4 Toward Real-Time SGG

This work proposes a novel architecture for real-time SGG, as shown in Figure 2c and Figure 2d. This architecture applies the Decoupled Two-Stage method, replacing the Faster-RCNN detector of PE-NET with a YOLO backbone (cf. Figure 2c). The Prototype Learning of PE-NET is improved by removing superfluous components, which results in Efficient Prototype Learning. This combination of DTS and Efficient Prototype Learning constitutes the REACT model. We also propose Dynamic Candidate Selection (DCS) to further reduce the latency of the proposed model at inference time, as described below.

**Decoupled Two-Stage SGG.** To maintain the object detector accuracy during relation prediction training, we propose to freeze the regression and the classification head of the object detector and perform NMS before the relation prediction stage. With this strategy, the object classifier in the relation prediction stage is also removed and class prediction from the object detector is used for the final prediction. Thus, the relation prediction stage outputs only the pairs and associate predicates, in contrast to also predicting the class labels of objects. The loss used during relation prediction:  $\mathcal{L}_{\text{total}} = \mathcal{L}_{\text{rel}} + \mathcal{L}_{\text{obj}}$ , then becomes:  $\mathcal{L}_{\text{total}} = \mathcal{L}_{\text{rel}}$ , lowering the model complexity and, consequently, its computational load. This approach helps to evaluate the context learning of SGG models independently of the object detector used. With this architecture, any object detector can be used in place of Faster-RCNN, without impacting stage 2 of the architecture. For instance, one could consider replacing Faster-RCNN with a real-time object detector such as YOLO [14]. To take advantage of YOLO versions, we leveraged the introduced Decoupled Two-Stage strategy and replaced the ResNeXt-101 backbone with YOLO’s CSPNet-based backbones [15, 16] (Figure 2c (a)). P5-FPN of Faster-RCNN was also replaced by the YOLOV8/9/10 PAN-FPN Necks (Figure 2c (b)). Finally, we removed the RPN and detection head of Faster-RCNN and replaced them with the YOLOV8/9/10 Detection Head (Figure 2c (c)). Unlike Faster-RCNN, YOLO-based architectures are not designed for feature extraction because they do not implement any ROI Align module. To address this issue, we combined the feature maps extracted from the P3, P4, and P5 layers of YOLO and added one 3x3 Conv block to reduce the feature sizes before ROI Align (Figure 2c (f)). The ROI Align module from Faster-RCNN has been modified to align features with corresponding bounding boxes at only three different scales (instead of five in the baseline implementation, Figure 2c (f)).

**Dynamic Candidate Selection.** Here, we introduce the DCS method to select an optimal number of proposal candidates at inference time. During training, the relation prediction stage takes as input a maximum amount of proposals  $\theta$  ( $\theta = 100$ ). During evaluation, we uniformly sample the number of proposals  $k$ , starting from 0. Using the generated slope for each metric, the optimal DCS threshold is computed as:  $x_{\text{opt}} = \min \{x \mid |f'(x)| < \varepsilon\}$ . During inference,  $x_{\text{opt}}$  is applied to control the maximum number of proposals to use as input for the relation prediction stage, successfully lowering the complexity of the task.

**Efficient Prototype Learning.** In PE-NET, node, and edge features are upsampled 8x and 4x respectively to a fixed size of 4096 by a feed-forward layer (steps (g) and (h) in Figure 2b). We believe this is unnecessary and that the model will perform similarly without upsampling. We then removed this layer and kept the original feature sizes of 256 and 512, respectively. In the latter stage during prototype learning, we removed the associated downsampling layers. For the PE-NET model, the use of union features for the edge representation seems redundant with the visual features of the subject and object. As a result, we removed the use of union features and dedicated ROI Align step (Figure 2a (d)). By doing so, the edge representation refinement step (Figure 2a (g)) can also be removed and the spa-

B	D	Relation Head	mR@20/50/100	R@20/50/100	F1@K	mAP <sup>50</sup>	Latency	Params
CSPDarkNet-53	YOLOv8m-DTS	REACT (ours) †	<u>18.3</u> / <u>20.0</u> / <u>20.8</u>	27.5 / 30.9 / 32.2	<u>23.9</u>	<b>53.1</b>	<u>23.0</u>	<u>43.3M</u>
		REACT (ours)	<b>18.3</b> / <b>20.1</b> / <b>20.9</b>	27.6 / 30.9 / 32.3	<b>23.9</b>	53.1	32.5	43.3M
		PE-NET † [10]	17.1 / 19.0 / 19.8	<u>28.0</u> / <u>31.3</u> / 32.9	23.2 †9.1	53.1 †17.6	51.7 †338	187M
		PE-NET [10]	17.1 / 19.0 / 19.9	<b>28.0</b> / <b>31.3</b> / <u>33.0</u>	23.2 †9.1	53.1 †17.6	103.0 †261	187M
		GPS-NET † [25]	10.9 / 12.6 / 13.5	26.3 / 30.0 / 31.8	17.3 †5.7	53.1 †21.5	27.8 †286	45.3M
		GPS-NET [25]	11.1 / 12.7 / 13.7	26.6 / 30.1 / 31.9	17.6 †5.9	53.1 †21.5	41.1 †272	45.3M
		Neural-Motifs † [10]	10.1 / 11.6 / 12.5	25.7 / 28.7 / 30.3	16.2 †3.8	53.1 †17.2	22.4 †296	52.9M
		Neural-Motifs [10]	10.1 / 11.6 / 12.5	25.7 / 28.7 / 30.4	16.2 †3.8	53.1 †17.2	35.8 †282	52.9M
		VCTree † [10]	10.7 / 12.2 / 12.9	22.1 / 25.3 / 26.8	16.1 †3.7	53.1 †20.5	183.2 †336	268.0M
		VCTree [10]	10.7 / 12.2 / 13.0	22.1 / 25.3 / 26.8	16.1 †3.8	53.1 †20.5	239.5 †280	268.0M
ResNeXt-101	Faster-RCNN	PE-NET [10]	10.7 / 11.7 / 12.0	16.8 / 18.7 / 19.5	14.1	35.5	390.4	426.5M
		GPS-NET [25]	8.2 / 8.8 / 9.2	15.7 / 18.1 / 19.2	11.7	31.6	313.9	391.6M
		Neural-Motifs [10]	8.9 / 9.6 / 9.8	16.9 / 18.7 / 19.5	12.5	<u>35.9</u>	318.6	369.6M
		VCTree [10]	7.9 / 9.1 / 9.6	18.0 / 20.7 / 22.3	12.4	32.6	519.5	365.9M
		Transformer [10]	7.6 / 8.2 / 8.5	16.2 / 17.9 / 18.7	11.1	34.6	296.2	328.3M
DETR		EGTR [10]	12.0 / 14.5 / 16.6	24.9 / 30.3 / <b>33.8</b>	19.4	33.6	78.3	<b>42.5M</b>
		RelTR [10]	7.9 / 10.0 / 11.7	12.9 / 17.3 / 20.2	12.4	25.7	59.6	63.7M

Table 2: Results on the PSG dataset. † represents evaluation with our DCS strategy. Bold and underlined represent the best and second best for each metric. ↓ and ↑ represent the improvements of DTS-YOLO against the corresponding baselines.

tial features fed directly to the context learning (Figure 2d (i)). To further boost accuracy, we proposed to modify the fusion of subject  $s$  and object  $o$  features during Prototype Learning of the PE-NET model. We replaced the fusion operation:  $ReLU(s + o) - (s - o)^2$  with a single linear layer and removed the subsequent gate operation.

## 5 Experiments

**Datasets.** In SGG, the most widely used dataset is Visual Genome [17]. The commonly used split of the data is called VG150 and contains annotations from the top 150 object classes and top 50 predicate classes. However, VG150 suffers from severe biases [8, 28, 10] and inherent issues such as the presence of ambiguous classes (e.g. the classes "people", "men" etc) [23, 10]. Recently, two new datasets have been proposed with higher-quality annotations: the PSG [10] and IndoorVG [27] datasets. Both datasets have been carefully annotated to remove the presence of ambiguous classes or wrong annotations, which makes them a better choice for benchmarking our approach.

**Metrics.** Following previous work [8, 39], we used the Recall@K (R@K) and mean-Recall@K (mR@K) metrics to measure the performance of models. For both metrics, we evaluate the recall on the top  $K$  ( $k = [20, 50, 100]$ ) relations predicted, ranked by confidence. The Recall@K evaluates the overall performance of a model on the selected dataset whereas meanRecall@K evaluates the performance on the average of all predicate classes, which is more significant for long-tail learning such as in the task of SGG. Both metrics are averaged in the F1@K metric as follows:  $F1@K = \frac{2 \times R@K \times mR@K}{R@K + mR@K}$  which efficiently represents

B	Relation Head	mR@K	R@K	F1@K	mAP <sup>50</sup>
DTS	REACT (ours)	<b>18.0</b>	<b>30.9</b>	<b>22.8</b>	<b>37.2</b>
	PE-NET	<u>16.0</u>	29.4	<u>20.7</u>	37.2
	GPS-NET	9.9	29.2	14.8	37.2
	Neural-Motifs	11.1	<u>30.5</u>	16.2	37.2
	VCTree	14.9	18.9	16.7	37.2
	Transformer	12.3	28.4	17.2	37.2
TS	PE-NET	13.8	27.1	18.1	25.2
	GPS-NET	6.7	11.9	8.6	17.4
	Neural-Motifs	9.8	15.2	11.9	<u>26.2</u>
	VCTree	11.0	14.7	12.6	25.5
	Transformer	9.9	16.8	12.5	24.2
OS	EGTR [10]	7.1	10.6	8.5	14.7
	RelTR [9]	7.7	11.4	9.2	14.1

Table 3: Results on IndoorVG. mR@K and R@K are average for  $k = [20, 50, 100]$ .

B	Model	mR@K	R@K	F1@K	mAP <sup>50</sup>
DTS	REACT	12.9	27.4	17.6	<b>31.8</b>
	PE-NET	13.3	32.6	<u>18.9</u>	29.2
TS	SQUAT [11]	<b>15.3</b>	26.7	<b>19.4</b>	-
	BGNN [12]	11.6	<u>33.4</u>	17.3	29.0
	VCTree	7.2	<b>33.9</b>	11.8	28.1
OS	EGTR [10]	7.8	29.3	12.4	<u>30.8</u>
	SGTR [13]	<u>13.6</u>	26.5	18.0	25.4
	SS-RCNN [14]	9.5	36.0	15.0	23.8
	RelTR [9]	8.0	24.3	12.0	26.4

Table 4: REACT compared to previous work on VG150 [17, 18] (reported results). mR@K and R@K are the average for  $k = [50, 100]$  as some approaches do not report  $k = 20$ .

the trade-off for the model performance between head and tail predictions. Object Detection (OD) accuracy is measured using standard mAP@50 (mAP<sup>50</sup>).

**Implementation details.** The latest YOLO versions (V8, V9, and V10) can be used interchangeably in our approach. For simplicity here, we will present experiments for the YOLOV8 medium version [15] (YOLOV8m). YOLOV8m has been trained for object detection for 100 epochs on all datasets with a batch size of 16 and image size 640x640. Relation prediction models have been trained for 20 epochs, batch size 8 with the SGD optimizer, and an initial learning rate of  $1e^{-3}$ . For Dynamic Candidate Selection (DCS), we choose  $\varepsilon = 1e^{-5}$ . Inference without DCS is performed with 100 proposals for all models. In contrast to YOLO, models trained with Faster-RCNN use 600x1000 image sizes. We fully re-trained seven different relation prediction models on the PSG and IndoorVG datasets: Neural-Motifs [4], VCTree [5], Transformer [6], GPS-Net [7], PE-NET [8], RelTR [9], and EGTR [10] following the provided codebases. All models are implemented without any re-weighting [5] or de-biasing strategy [6]. Latency is benchmarked with a batch size of 1<sup>1</sup>.

**Results.** In Table 2 and Table 3 we display the performance of our DTS architecture in OD accuracy compared to previous work. The F1@K results from Table 2 are represented as a graph in Figure 1. In the text, we refer to improvements as mean absolute percentage. By using YOLOV8, we improved the mAP by 54.37% on the PSG dataset (Table 2) and 69.92% on IndoorVG (Table 3), compared to TS approaches with Faster-RCNN. Compared to OS approaches (EGTR [9] and RelTR [9]), mAP is improved by 120% on average, which demonstrates the inefficiency of such approaches for the OD task. For a fair comparison, we also present the performance of the REACT model on the VG150 dataset, see Table 4. The performance of REACT in mAP is better by one point than the best approach EGTR. We believe that the low quality of the bounding box annotations and the ambiguous classes in VG150 are confusing the YOLOV8 detector, which leads to only a small improvement against Faster-RCNN. On the PSG dataset, we experienced an average improvement of 58.47% in F1@k by using our DTS method compared to the same approaches with Faster-RCNN. In addition, our REACT model outperforms the PE-NET model with DTS by a small margin (23.9 versus 23.2 in F1@K). We observe that the gain in F1@k is not very strongly

<sup>1</sup>Hardware used: 11th Gen Intel™ Core™ i9-11950H @ 2.60GHz x 16, NVIDIA GeForce RTX 3080 Laptop GPU 16GB VRAM, 2 x 16GB 3200 MHz RAM.

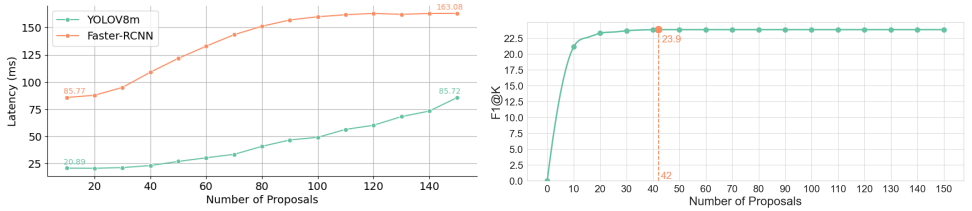


Figure 3: Left: Latency for the REACT model using a different number of proposals per image, with batch size 1. Right: Average F1@k for the REACT model with DTS-YOLO.

correlated to the gain in mAP between the Two-Stage and DTS approaches, as we measured a correlation coefficient of 0.75 between the two. On the IndoorVG dataset, we observe an improvement of 38.76% in F1@K with the DTS approach. Our REACT model also outperforms PE-NET (DTS) by a strong margin (22.8 versus 20.7 in F1@K). We observe that REACT outperforms some Two-Stage approaches (Motifs, VCTree, and BGNN) for RelPred on VG150 (see Table 4) but is not competitive with more recent approaches (PE-NET and SQUAT). We believe this is due to noisy feature representation. Because REACT has fewer parameters, it is more sensitive to noisy data. Regarding latency, we demonstrated an improvement of 84.99% using YOLOV8 instead of Faster-RCNN, which is a considerable gap. Regarding the number of parameters, the DTS approach uses on average 77.47% less parameters than the baseline. Our introduced REACT model is the fastest one, with a latency of 32.5ms. By applying our DCS strategy, we gain an average of 66.5% latency on all models (compared to the YOLOV8m-DTS versions) with a relative average loss of 1% in F1@K. The EGTR model stays the best overall in terms of parameter count by a slow margin (42.5M versus 43.3M for REACT). By comparing REACT to the fastest model benchmarked, RelTR [24], REACT is 2.7x faster with +10 points on average in F1@K and +24.9 points on average in mAP<sup>50</sup> for the 3 datasets. By taking into account OD accuracy, RelPred accuracy, and latency, our REACT model is the best compromise. Even for the VG150 dataset, REACT is a better choice because no other two-stage approaches are close to real-time inference. On the other hand, when evaluated fairly, one-stage approaches are clearly behind in terms of mAP and F1@K on all datasets, and are then not a good choice in comparison to REACT.

**Latency and Number of Proposals.** As explained before, the second stage of SGG takes as input a fixed number of  $n$  proposals as node candidates. There could be a maximum of  $n * (n - 1)$  possible pairs in the graph, thus when doing matching the computational complexity is supposed to scale accordingly. To demonstrate this hypothesis, we evaluated the performance of the REACT model in both latency and accuracy for different numbers of input proposals  $k = \{10, 150\}$  with DTS-YOLOV8 and with classical Faster-RCNN. For all experiments, we ranked proposals by confidence of the backbone and selected the top  $k$ . The results of these experiments are shown in fig. 3 (top), where we observe a plateau phenomenon for REACT with Faster-RCNN above 100 proposals. This behavior does not appear when using DTS+YOLOV8. By using 150 proposals with DTS+YOLOV8, the latency was similar to 10 proposals with Faster-RCNN. The evaluation of the REACT model under different sampling conditions with our DCS strategy is represented in fig. 3 (bottom). In this figure, we can see that the optimal value was found at 23.89 for  $k = 42$ , just before that the performance starts to be saturated.

**Features Fusion.** During context learning of the REACT model, and more generally in a lot of approaches in SGG [25, 63, 43, 42], different feature sources are used to model the

T	V	S	U	mR@K	R@K	F1@K	Latency	Params
✓	✓	✓	✓	14.6	<b>30.8</b>	19.8	36.0	42.7M
✓	✓	✓	✗	<b>19.7</b>	<u>30.2</u>	<b>23.9</b>	32.5	42.7M
✓	✓	✗	✓	14.2	29.9	19.3	27.3	42.7M
✓	✓	✗	✗	14.5	30.1	19.6	<u>18.5</u>	<u>36.6M</u>
✓	✗	✗	✗	13.5	29.1	18.4	<b>16.2</b>	<b>35.2M</b>

Table 5: Feature sources experiments. V and T are visual and textual features for  $\langle \text{subject}, \text{object} \rangle$ , and S and U are Spatial and Union features, respectively.

edge representation. First, union and spatial features are combined and then merged with the addition of the subject and object node features. The node features are created using visual and textual features obtained for each proposal. In our REACT model, we removed the dependency on the union features (see Figure 2d (i)). In the following, we justify our choice by analyzing the impact of each feature type on learning. The results from these experiments are displayed in Table 5. The baseline REACT model is the second row. With union features (first row) we observe a significant decrease in F1@K as well as latency. We hypothesize that union features are too noisy and confuse the model. This is consistent with previous work which highlights the importance of spatial features for the task [12]. In the last two rows, we removed all dependencies on contextual features (union and spatial) and kept only the concatenation of the subject and object node as initial edge features. We observe only a slight decrease by keeping only text features (last row). In fact, the model can retain up to 71% of the optimal performance by learning only from the textual GLoVe features. This suggests a trade off between text and visual features in the task.

## 6 Conclusion

In this work, we proposed a novel implementation of a real-time Scene Graph Generation model that attains competitive performance with a latency of 23ms. We proposed a new architecture, the Decoupled Two-Stage SGG (DTS), aiming at taking advantage of real-time object detectors for SGG. We also proposed a new inference method, Dynamic Candidate Selection (DCS) to further reduce latency by 66.5% on average without compromising performance. Finally, we proposed a new model, REACT, which combines the DTS architecture with efficient prototype learning for lower latency and improved accuracy. Our main finding is that the performance and latency of SGG models are heavily correlated with the quality and quantity of object proposals generated by the object detector. However, regarding both overall performance and latency, a trade-off can be found by using our DCS strategy. Another finding is the over-reliance of models on the text features for relation prediction. Future work will consider implementing the REACT model in constraint settings such as embodied agent navigation or reasoning. Due to its small size, REACT can be embedded onboard robotic platforms and provide reliable and fast predictions that can foster reasoning.

## Acknowledgments

This work has been supported by the Brittany Region and the Knut and Alice Wallenberg foundation and the Wallenberg AI, Autonomous Systems and Software Program (WASP).

## References

- [1] Nicolas Carion, Francisco Massa, Gabriel Synnaeve, Nicolas Usunier, Alexander Kirillov, and Sergey Zagoruyko. End-to-end object detection with transformers. In *European conference on computer vision*, pages 213–229. Springer, 2020.
- [2] Xiaojun Chang, Pengzhen Ren, Pengfei Xu, Zhihui Li, Xiaojiang Chen, and Alex Hauptmann. A Comprehensive Survey of Scene Graphs: Generation and Application. *IEEE Transactions on Pattern Analysis and Machine Intelligence*, 45(1):1–26, January 2023. ISSN 0162-8828, 2160-9292, 1939-3539. doi: 10.1109/TPAMI.2021.3137605.
- [3] Yuren Cong, Michael Ying Yang, and Bodo Rosenhahn. ReTR: Relation Transformer for Scene Graph Generation, August 2022.
- [4] Yuren Cong, Michael Ying Yang, and Bodo Rosenhahn. ReTR: Relation Transformer for Scene Graph Generation, August 2022. arXiv:2201.11460 [cs] version: 2.
- [5] Vinay Damodaran, Sharanya Chakravarthy, Akshay Kumar, Anjana Umamathy, Teruko Mitamura, Yuta Nakashima, Noa Garcia, and Chenhui Chu. Understanding the role of scene graphs in visual question answering. *arXiv preprint arXiv:2101.05479*, 2021.
- [6] Xingning Dong, Tian Gan, Xueming Song, Jianlong Wu, Yuan Cheng, and Liqiang Nie. Stacked Hybrid-Attention and Group Collaborative Learning for Unbiased Scene Graph Generation. In *2022 IEEE/CVF Conference on Computer Vision and Pattern Recognition (CVPR)*, pages 19405–19414, New Orleans, LA, USA, June 2022. IEEE. ISBN 978-1-66546-946-3. doi: 10.1109/CVPR52688.2022.01882.
- [7] Samir Yitzhak Gadre, Kiana Ehsani, Shuran Song, and Roozbeh Mottaghi. Continuous scene representations for embodied ai. In *Proceedings of the IEEE/CVF Conference on Computer Vision and Pattern Recognition*, pages 14849–14859, 2022.
- [8] Drew A. Hudson and Christopher D. Manning. GQA: A New Dataset for Real-World Visual Reasoning and Compositional Question Answering, May 2019.
- [9] Jinbae Im, JeongYeon Nam, Nokyung Park, Hyungmin Lee, and Seunghyun Park. Egrt: Extracting graph from transformer for scene graph generation. *arXiv preprint arXiv:2404.02072*, 2024.
- [10] Jinbae Im, JeongYeon Nam, Nokyung Park, Hyungmin Lee, and Seunghyun Park. EGTR: Extracting Graph from Transformer for Scene Graph Generation, April 2024.
- [11] Tianlei Jin, Fangtai Guo, Qiwei Meng, Shiqiang Zhu, Xiangming Xi, Wen Wang, Zonghao Mu, and Wei Song. Fast Contextual Scene Graph Generation With Unbiased Context Augmentation. In *Proceedings of the IEEE/CVF Conference on Computer Vision and Pattern Recognition*, pages 6302–6311, 2023.
- [12] Tianlei Jin, Fangtai Guo, Qiwei Meng, Shiqiang Zhu, Xiangming Xi, Wen Wang, Zonghao Mu, and Wei Song. Fast Contextual Scene Graph Generation With Unbiased Context Augmentation. pages 6302–6311, 2023.

- [13] Tianlei Jin, Wen Wang, Shiqiang Zhu, Xiangming Xi, Qiwei Meng, Zonghao Mu, and Wei Song. Independent Relationship Detection for Real-Time Scene Graph Generation. In Mohammad Tanveer, Sonali Agarwal, Seiichi Ozawa, Asif Ekbal, and Adam Jatowt, editors, *Neural Information Processing*, Communications in Computer and Information Science, pages 106–118, Singapore, 2023. Springer Nature. ISBN 978-981-9916-39-9. doi: 10.1007/978-981-99-1639-9\_9.
- [14] Glenn Jocher. YOLOv5 by Ultralytics, May 2020. URL <https://github.com/ultralytics/yolov5>.
- [15] Glenn Jocher, Ayush Chaurasia, and Jing Qiu. Ultralytics YOLO, January 2023. URL <https://github.com/ultralytics/ultralytics>.
- [16] Deunsol Jung, Sanghyun Kim, Won Hwa Kim, and Minsu Cho. Devil’s on the edges: Selective quad attention for scene graph generation. In *Proceedings of the IEEE/CVF Conference on Computer Vision and Pattern Recognition*, pages 18664–18674, 2023.
- [17] Ranjay Krishna, Yuke Zhu, Oliver Groth, Justin Johnson, Kenji Hata, Joshua Kravitz, Stephanie Chen, Yannis Kalantidis, Li-Jia Li, David A. Shamma, Michael S. Bernstein, and Li Fei-Fei. Visual Genome: Connecting Language and Vision Using Crowdsourced Dense Image Annotations. *International Journal of Computer Vision*, 123(1):32–73, May 2017. ISSN 1573-1405. doi: 10.1007/s11263-016-0981-7.
- [18] Rongjie Li, Songyang Zhang, Bo Wan, and Xuming He. Bipartite Graph Network with Adaptive Message Passing for Unbiased Scene Graph Generation. In *2021 IEEE/CVF Conference on Computer Vision and Pattern Recognition (CVPR)*, pages 11104–11114, Nashville, TN, USA, June 2021. IEEE. ISBN 978-1-66544-509-2. doi: 10.1109/CVPR46437.2021.01096.
- [19] Rongjie Li, Songyang Zhang, and Xuming He. SGTR: End-to-end Scene Graph Generation with Transformer. In *2022 IEEE/CVF Conference on Computer Vision and Pattern Recognition (CVPR)*, pages 19464–19474, New Orleans, LA, USA, June 2022. IEEE. ISBN 978-1-66546-946-3. doi: 10.1109/CVPR52688.2022.01888.
- [20] Rongjie Li, Songyang Zhang, and Xuming He. SGTR+: End-to-end Scene Graph Generation with Transformer, January 2024.
- [21] Xinghang Li, Di Guo, Huaping Liu, and Fuchun Sun. Embodied semantic scene graph generation. In *Conference on robot learning*, pages 1585–1594. PMLR, 2022.
- [22] Weixin Liang, Yanhao Jiang, and Zixuan Liu. GraghVQA: Language-Guided Graph Neural Networks for Graph-based Visual Question Answering. In Amir Zadeh, Louis-Philippe Morency, Paul Pu Liang, Candace Ross, Ruslan Salakhutdinov, Soujanya Poria, Erik Cambria, and Kelly Shi, editors, *Proceedings of the Third Workshop on Multimodal Artificial Intelligence*, pages 79–86, Mexico City, Mexico, June 2021. Association for Computational Linguistics. doi: 10.18653/v1/2021.maiworkshop-1.12.
- [23] Yuanzhi Liang, Yalong Bai, Wei Zhang, Xueming Qian, Li Zhu, and Tao Mei. VrRVG: Refocusing Visually-Relevant Relationships. In *2019 IEEE/CVF International Conference on Computer Vision (ICCV)*, pages 10402–10411, Seoul, Korea (South), October 2019. IEEE. ISBN 978-1-72814-803-8. doi: 10.1109/ICCV.2019.01050.

- [24] Tsung-Yi Lin, Piotr Dollár, Ross Girshick, Kaiming He, Bharath Hariharan, and Serge Belongie. Feature pyramid networks for object detection. In *Proceedings of the IEEE conference on computer vision and pattern recognition*, pages 2117–2125, 2017.
- [25] Xin Lin, Changxing Ding, Jinquan Zeng, and Dacheng Tao. GPS-Net: Graph Property Sensing Network for Scene Graph Generation. In *2020 IEEE/CVF Conference on Computer Vision and Pattern Recognition (CVPR)*, pages 3743–3752, Seattle, WA, USA, June 2020. IEEE. ISBN 978-1-72817-168-5. doi: 10.1109/CVPR42600.2020.00380.
- [26] Cewu Lu, Ranjay Krishna, Michael Bernstein, and Li Fei-Fei. Visual Relationship Detection with Language Priors. In Bastian Leibe, Jiri Matas, Nicu Sebe, and Max Welling, editors, *Computer Vision – ECCV 2016*, pages 852–869, Cham, 2016. Springer International Publishing. ISBN 978-3-319-46448-0. doi: 10.1007/978-3-319-46448-0\_51.
- [27] Maëlic Neau, Paulo Santos, Anne-Gwenn Bosser, and Cédric Buche. In defense of scene graph generation for human-robot open-ended interaction in service robotics. In *Robot World Cup*, pages 299–310. Springer, 2023.
- [28] Maëlic Neau, Paulo E Santos, Anne-Gwenn Bosser, and Cédric Buche. Fine-grained is too coarse: A novel data-centric approach for efficient scene graph generation. In *Proceedings of the IEEE/CVF International Conference on Computer Vision*, pages 11–20, 2023.
- [29] Kien Nguyen, Subarna Tripathi, Bang Du, Tanaya Guha, and Truong Q. Nguyen. In Defense of Scene Graphs for Image Captioning. In *Proceedings of the IEEE/CVF International Conference on Computer Vision*, pages 1407–1416, 2021.
- [30] Jeffrey Pennington, Richard Socher, and Christopher D Manning. Glove: Global vectors for word representation. In *Proceedings of the 2014 conference on empirical methods in natural language processing (EMNLP)*, pages 1532–1543, 2014.
- [31] Shaoqing Ren, Kaiming He, Ross Girshick, and Jian Sun. Faster r-cnn: Towards real-time object detection with region proposal networks. *Advances in neural information processing systems*, 28, 2015.
- [32] Kaihua Tang, Hanwang Zhang, Baoyuan Wu, Wenhan Luo, and Wei Liu. Learning to Compose Dynamic Tree Structures for Visual Contexts. In *2019 IEEE/CVF Conference on Computer Vision and Pattern Recognition (CVPR)*, pages 6612–6621, Long Beach, CA, USA, June 2019. IEEE. ISBN 978-1-72813-293-8. doi: 10.1109/CVPR.2019.00678.
- [33] Kaihua Tang, Yulei Niu, Jianqiang Huang, Jiaxin Shi, and Hanwang Zhang. Unbiased Scene Graph Generation From Biased Training. In *2020 IEEE/CVF Conference on Computer Vision and Pattern Recognition (CVPR)*, pages 3713–3722, Seattle, WA, USA, June 2020. IEEE. ISBN 978-1-72817-168-5. doi: 10.1109/CVPR42600.2020.00377.
- [34] Yao Teng and Limin Wang. Structured sparse r-cnn for direct scene graph generation. In *Proceedings of the IEEE/CVF Conference on Computer Vision and Pattern Recognition*, pages 19437–19446, 2022.

- [35] Yao Teng and Limin Wang. Structured Sparse R-CNN for Direct Scene Graph Generation. In *2022 IEEE/CVF Conference on Computer Vision and Pattern Recognition (CVPR)*, pages 19415–19424, New Orleans, LA, USA, June 2022. IEEE. ISBN 978-1-66546-946-3. doi: 10.1109/CVPR52688.2022.01883.
- [36] Ao Wang, Hui Chen, Lihao Liu, Kai Chen, Zijia Lin, Jungong Han, and Guiguang Ding. Yolov10: Real-time end-to-end object detection. *arXiv preprint arXiv:2405.14458*, 2024.
- [37] Chien-Yao Wang, I-Hau Yeh, and Hong-Yuan Mark Liao. Yolov9: Learning what you want to learn using programmable gradient information. *arXiv preprint arXiv:2402.13616*, 2024.
- [38] Dalin Wang, Daniel Beck, and Trevor Cohn. On the Role of Scene Graphs in Image Captioning. In Aditya Mogadala, Dietrich Klakow, Sandro Pezzelle, and Marie-Francine Moens, editors, *Proceedings of the Beyond Vision and LANGUAGE: inTEgrating Real-world kNOWLEDGE (LANTERN)*, pages 29–34, Hong Kong, China, November 2019. Association for Computational Linguistics. doi: 10.18653/v1/D19-6405.
- [39] Danfei Xu, Yuke Zhu, Christopher B. Choy, and Li Fei-Fei. Scene Graph Generation by Iterative Message Passing. In *Proceedings of the IEEE Conference on Computer Vision and Pattern Recognition*, pages 5410–5419, 2017.
- [40] Jianwei Yang, Jiasen Lu, Stefan Lee, Dhruv Batra, and Devi Parikh. Graph R-CNN for Scene Graph Generation. In Vittorio Ferrari, Martial Hebert, Cristian Sminchisescu, and Yair Weiss, editors, *Computer Vision – ECCV 2018*, volume 11205, pages 690–706. Springer International Publishing, Cham, 2018. ISBN 978-3-030-01245-8 978-3-030-01246-5. doi: 10.1007/978-3-030-01246-5\_41. Series Title: Lecture Notes in Computer Science.
- [41] Jingkan Yang, Yi Zhe Ang, Zujin Guo, Kaiyang Zhou, Wayne Zhang, and Ziwei Liu. Panoptic Scene Graph Generation. In Shai Avidan, Gabriel Brostow, Moustapha Cissé, Giovanni Maria Farinella, and Tal Hassner, editors, *Computer Vision – ECCV 2022*, Lecture Notes in Computer Science, pages 178–196, Cham, 2022. Springer Nature Switzerland. ISBN 978-3-031-19812-0. doi: 10.1007/978-3-031-19812-0\_11.
- [42] Xuewen Yang, Yingru Liu, and Xin Wang. Reformer: The relational transformer for image captioning. In *Proceedings of the 30th ACM International Conference on Multimedia*, pages 5398–5406, 2022.
- [43] Rowan Zellers, Mark Yatskar, Sam Thomson, and Yejin Choi. Neural Motifs: Scene Graph Parsing with Global Context. In *2018 IEEE/CVF Conference on Computer Vision and Pattern Recognition*, pages 5831–5840, Salt Lake City, UT, June 2018. IEEE. ISBN 978-1-5386-6420-9. doi: 10.1109/CVPR.2018.00611.
- [44] Chaofan Zheng, Xinyu Lyu, Lianli Gao, Bo Dai, and Jingkuan Song. Prototype-based embedding network for scene graph generation. In *Proceedings of the IEEE/CVF Conference on Computer Vision and Pattern Recognition*, pages 22783–22792, 2023.

# Supplementary Material

## REACT: Real-time Efficiency and Accuracy Compromise for Tradeoffs in Scene Graph Generation

Maëlic Neau<sup>1,3,4 †</sup>  
maelic.neau@umu.se

Paulo E. Santos<sup>2,3</sup>  
paulo.santos@priorianalytica.com

Anne-Gwenn Bosser<sup>4</sup>  
bossier@enib.fr

Cédric Buche<sup>5,6</sup>  
cedric.buche@cnrs.fr

Akihiro Sugimoto<sup>7</sup>  
sugimoto@nii.ac.jp

<sup>1</sup> Umeå University, Universitetstorget 4,  
Umeå, Sweden

<sup>2</sup> PrioriAnalytica, 74 Pirie St, Adelaide,  
Australia

<sup>3</sup> Flinders University, Sturt Rd, Bedford  
Park, Australia

<sup>4</sup> Bretagne INP - ENIB, 945 Av. du  
Technopôle, Plouzané, France

<sup>5</sup> CNRS IRL 2010 CROSSING, 11 Victo-  
ria Drive, Adelaide, Australia

<sup>6</sup> IMT Atlantique, 655 Av. du Technopôle,  
Plouzané, France

<sup>7</sup> National Institute of Informatics, 2-12 Hi-  
totsubashi, Tokyo, Japan

---

## A Datasets

### A.1 VG150 Annotations Biases

The VG150 dataset has become the main benchmark for Scene Graph Generation. This dataset has been extracted from the original Visual Genome (VG) annotations. In their work, Xu et al. [11] proposed to select the top 150 objects and top 50 predicate classes from VG to compose the VG150 dataset. However, in this process, no manual refinement has been performed to verify the coherence of the data. The original Visual Genome annotations are known to be very noisy [14] with a lot of interchangeable classes. In table 1 we display some of the classes of the VG150 dataset. For every column, we can see that all classes from subsequent rows can be used interchangeably with the label from the first row. This leads to strong confusion of (1) the object detector and (2) the relation predictor.

In Figure 1 we display the confusion matrix for the YOLOV8-medium model trained on VG150. We can clearly observe confusion between the class "man", "boy" and "person" or another confusion between "airplane" and "plane" which demonstrates the low quality of

Objects			Predicates	
person	animal	vehicle	wears	on
girl	dog	car	wearing	on top of
woman	bear	truck		above
man	cat	train		

Table 1: Confused classes of VG150.

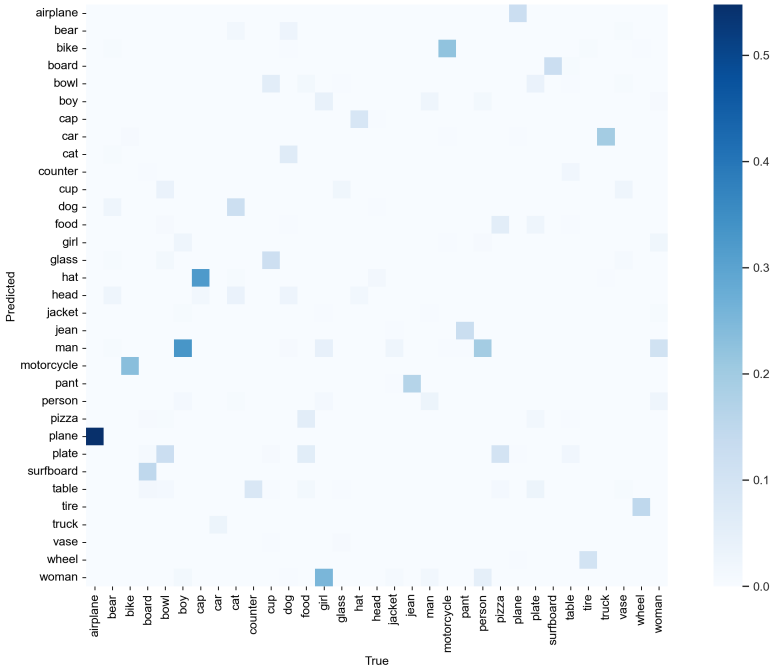


Figure 1: Normalized confusion matrix for the YOLOV8-m model on VG150. For convenience, we only display values above 0.1.

annotations. As a result, we decided not to compare our approach to the VG150 dataset. We still report the results of the REACT model on the VG150 dataset to compare with approaches that cannot be retrained on more qualitative datasets.

## A.2 Other Datasets

In addition, we choose not to compare our approach on the GQA [1] and OpenImage [4] datasets. The rationale is as follows: the GQA dataset is also a split of Visual Genome and thus contains the same biases as VG150 [12]. In addition, GQA contains 301 predicate classes with a lot of them being ambiguous or that can be used interchangeably (such as "standing" and "standing on", etc...). The OpenImage dataset contains only very sparse annotations (an average of 2.7 relations per image), which is not tailored for SGG. In addition, it includes a lot of noisy object classes with only a few samples each. Another issue with OpenImage is the diversity of relations. In fact, more than 60% of the subject-object pairs are only associated with a single predicate (for instance,  $\langle person, guitar \rangle$  is always associated

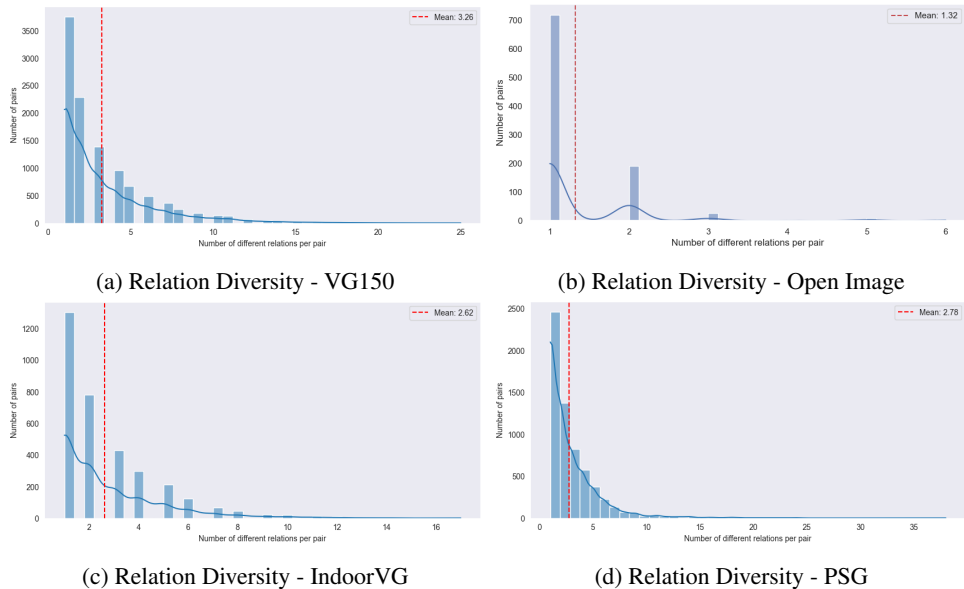


Figure 2: Comparison of the number of different predicates annotated for each  $\langle \text{subject}, \text{object} \rangle$  pair in SGG datasets.

with the predicate *playing*), see Figure 2. This imbalance will result in a strong overfitting of SGG models. These models will likely learn strict correlations on the linguistic features of the subject and object rather than any meaningful visual interpretation of the relation. VG150, OpenImage, and GQA are all heavily long-tailed datasets. Our work does not focus on long-tail learning [8], in consequence, we report our main results on the PSG and IndoorVG datasets which are less biased toward tail classes. In addition, these datasets have more qualitative annotations with no spurious or ambiguous classes. For the IndoorVG dataset, we used the V4 version provided in the authors’ codebase. In Table 2 you can find a comparison of each dataset.

Dataset	Images	Obj.	Pred.	# Rel.	Rel/Img
VG150 [3]	108,073	150	50	622,705	5.76
OpenImage [4]	133,503	601	30	367,914	2.75
GQA [1]	85,638	200	310	471,614	5.51
PSG [12]	48,749	133	56	278,356	5.71
IndoorVG [6]	14,674	83	34	112,804	7.69

Table 2: Comparison of different Scene Graph datasets, # Rel. displays the total number of relationships and Rel/Img the average number of relations per image.

Model	mAP <sup>50</sup>	mR@K	R@K	F1@K	Lat.	Params
YOLOV8	53.1	<b>19.7</b>	<u>30.2</u>	<b>23.9</b>	<b>32.5</b>	42.7M
YOLOV9	53.3	16.3	29.8	21.0	46.5	39.7M
YOLOV10	<b>54.5</b>	<u>16.9</u>	<b>33.0</b>	<u>22.3</u>	55.3	<b>33.4M</b>

Table 3: Performance of the REACT model using different object detectors with the DTS architecture. We used the medium version of each detector.

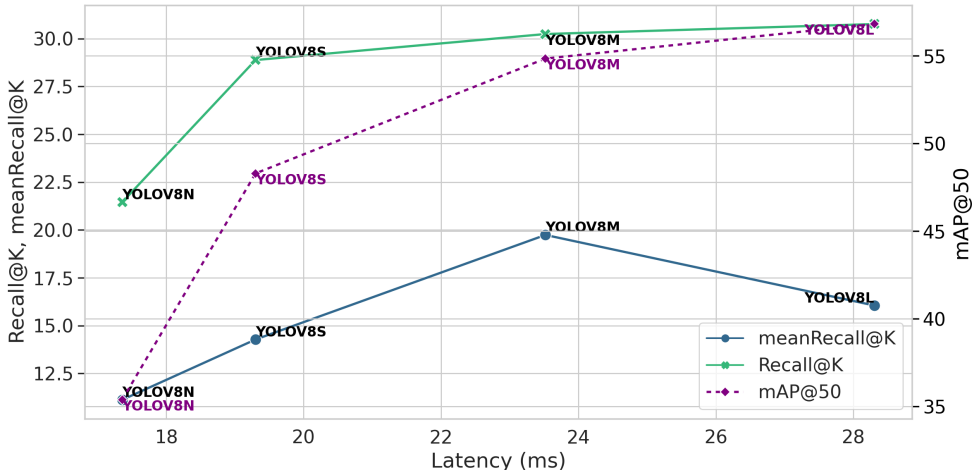


Figure 3: Average Recall@K, meanRecall@K, and mAP@50 performance for REACT with DCS against the corresponding latency using different variants of the YOLOV8 model.

## B Additional Experiments

### B.1 YOLO Versions Comparison

In the following, we compare the performance of our REACT model with different YOLO models for feature extraction and object detection. Similar to YOLOV8, we trained the YOLOV9-medium [10] and YOLOV10-medium [9] models on the PSG dataset [12] with batch size 8 for 100 epochs. Then, the REACT model has been trained for 20 epochs using the same hyperparameters as for YOLOV8. Results are displayed in Table 3. We observe no significant improvements in mR@K or R@K by using YOLOV9 or V10 in comparison to V8. The performance of YOLOV9 and YOLOV10 in object detection is superior to YOLOV8, by 0.2 and 1.4 points in mAP, respectively. Interestingly, the overall latency is worse for YOLOV10 and YOLOV9 than by using YOLOV8, which contradicts findings by the respective authors [9, 10]. For YOLOV9, we believe this could come from the size of the feature maps extracted from the backbone which is different than YOLOV8 (YOLOV9m uses a GELAN architecture with an output size of 240, whereas YOLOV8 output size is 192). Higher feature sizes will lead to more computation in the following stages as the subject and object visual representation will be based on these features.

Model	Motifs		PE-NET		Transformer	
	mR@K	R@K	mR@K	R@K	mR@K	R@K
<b>Union</b>	11.4	28.3	18.7	30.8	12.3	26.7
<b>No Union</b>	11.4	30.8	17.8	31.4	11.6	26.7

Table 4: Additional experiments with union features - PSG dataset.

## B.2 Scaling Down YOLOV8

To better evaluate the impact of the object detector accuracy on the relation prediction stage, we ran a set of experiments using different variants of YOLOV8 with the REACT model for Scene Graph Generation. Here, we trained the model with the same hyperparameters as before, only modifying the input size of the visual features used for relation prediction to match the different output channel sizes for each YOLOV8 variant. The results are displayed in Figure 3. We observed a strong correlation between mAP@50 and R@K (correlation coefficient = 0.97), and a correlation between mAP@50 and mR@K (correlation coefficient = 0.86). The performance of the larger model, YOLOV8-L is slightly worse in mR@K than the medium YOLOV8-M. We believe that the higher number of dimensions in the features extracted from the backbone could lead to more difficulties for the relation prediction training to converge. In addition, we observed a linear increase in latency with the size of the model. The performance of REACT with the smaller model, YOLOV8-N, is equivalent to the original PE-NET model on the PSG dataset but 22x faster and with 32x fewer parameters (426.5M versus 13.25M). In terms of the overall performance, the medium version seems to be the best. It has a good trade-off between all metrics and latency, making it a good choice for high performance in edge settings.

## B.3 Union Features

In the case of the proposed REACT model, our experiments show that the union features do not significantly contribute to the overall performance. Table 4 verifies this fact, where we observe that the union features are only beneficial in two out of six measures. This behavior is due to the fact that union features also provide extensive noise to the model which contributes negatively to their supposed beneficial effect. Recent work also reports that the textual and spatial features are the most important features for Two-Stage models [2].

## B.4 Detailed Latency

In the following, we detail the latency of each component of the Two-Stage and Decoupled Two-Stage architectures. Before feeding images to the model, some pre-processing is required (mainly image Transforms). To generate the final predictions, post-process is applied to convert class labels to names and rescale bounding boxes to the original image size. In Table 5 we display these values as well as a detail of the latency of the object detector (feature extraction + object detection) and the relation predictor. In addition, we display the minimum and maximum values obtained on the PSG dataset test set. Very low values account for no bounding box detected and high values for the maximum of 100 bounding boxes detected. We observe significant differences in latency for the relation prediction stage while object detection stays relatively similar for all models. The difference between max and min values

B	Model	Latency (ms)				Min	Max
		Pre-process	Obj. Det.	Rel. Pred.	Post-process		
DTS	REACT	0.60	16.08	15.70	0.53	19.40	55.36
	PE-NET	0.60	17.18	81.42	0.78	25.14	199.54
	GPS-NET	0.64	15.31	22.06	0.57	17.17	105.30
	Neural-Motifs	0.60	14.82	19.68	0.57	14.00	115.01
	VCTree	0.60	16.20	416.47	0.61	63.89	591.94
	Transformer	0.57	14.94	17.31	0.51	17.33	138.74
TS	PE-NET	0.97	91.35	287.63	0.62	118.09	1625.90
	GPS-NET	0.95	86.10	223.75	0.55	105.83	1325.97
	Neural-Motifs	1.01	86.19	224.96	0.53	113.87	1373.58
	VCTree	0.99	82.10	320.77	0.51	127.54	1583.71
	Transformer	0.94	85.20	201.00	0.53	105.96	1308.07

Table 5: Details of the latency for each model. The Min and Max correspond to the min and max values of the full forward pass of the model (without pre and post-process).

Model	REACT		PE-NET		GPS-Net		VCTree	
	DTS	TS	DTS	TS	DTS	TS	DTS	TS
<b>GFLOP</b>	176	7,067	700	7,901	233	5,006	493	4,757

Table 6: FLOP comparison for the different models on the test set of the PSG dataset.

for DTS is 7.91x whereas for TS models it is 12.67x. In addition to a more lightweight backbone, this difference demonstrates that our DTS method is able to remove computation from the relation prediction head. The significant range between minimum and maximum latency is an important parameter that needs to be accounted for deployment. Our REACT model has the lowest difference between min and max values, with 2.85x, showing that our relation head is the most efficient for real-time constraints.

## B.5 Complexity

In Table 6 we compare the Floating Point Operations per Second (FLOPs) for the models tested, using  $n = 100$  for the number of proposals. We observe a 10x to 40x improvement in FLOPs using DTS instead of TS. It is important to notice here that the number of FLOPs for Two-Stage approaches can vary depending on the image. For some images, the Region Proposal Network of Faster-RCNN will not be able to generate up to 100 proposals. In that case, a lower number of pairs will be created, and the relations prediction stage will take fewer FLOPs. The numbers here are then an average of the test set of the PSG dataset.

## C Dynamic Candidate Selection

### C.1 Rationale

In the Object Detection task, a confidence threshold is traditionally selected at inference time to control the quality of output bounding boxes. The paradigm of SGG leverages an Object Detection component, however, applying a set threshold to control the number of predicted proposals before the relation prediction stage is not desirable. First, the Two-Stage approaches rely on a separate classifier to decode the box labels after the relation predic-

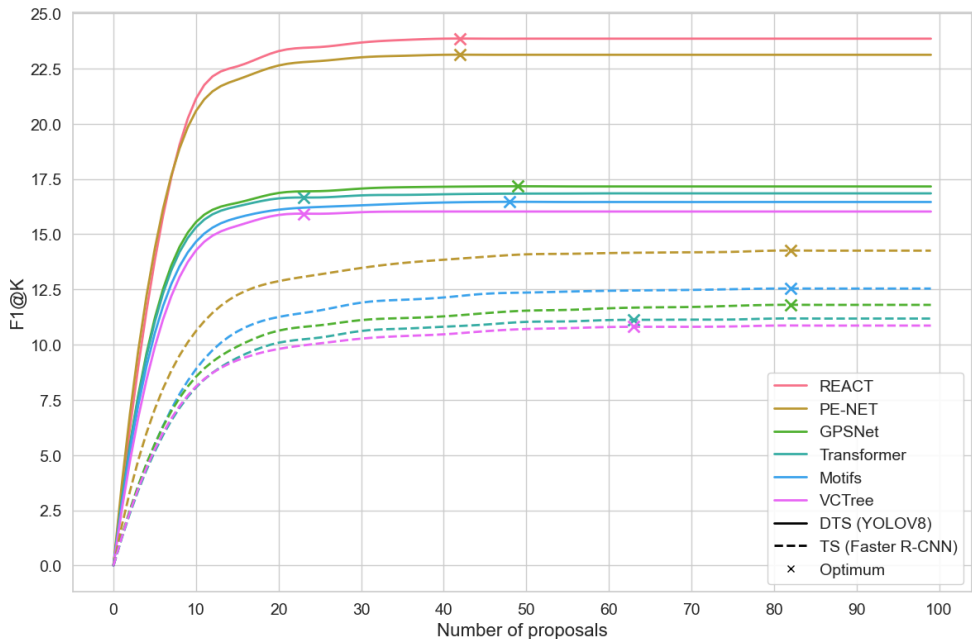


Figure 4: Comparison of Two-Stage and Decoupled Two-Stage architectures with our DCS strategy for inference.

tion stage. The performance of this classifier will impact the final score of the predicted proposals. Second, setting a hard threshold for object detection in our DTS approach will significantly affect the performance concerning relation prediction as the metrics used are not based on precision but rather recall ( $R@K$  and  $mR@K$ ). This will then be unfair when compared with the two-stage approaches. As a result, controlling the number of input proposals by using a saturation threshold for all models (i.e. our DCS strategy) seems more promising.

## C.2 Models Comparison

In this section, we present an in-depth analysis of the DCS strategy. In addition to Decoupled Two-Stage models, we ran evaluation on Two-Stage architectures with Faster-RCNN and DCS on the PSG dataset, results are displayed in Figure 4. We plot the optimum value found for each model. We observe that the optimum for Two-Stage models is significantly higher than for Decoupled Two-Stage models. The average optimum for TS is 74, while for DTS it is 37. This difference can be explained by the low quality of the bounding box predicted by the Faster-RCNN in Two-Stage architectures.

## D Training Details

All models are trained using `torch.use_deterministic_algorithms` as well as a set seed for all random variables. In Table 7 we display the hyperparameters used for all training of Two-Stage and Decoupled Two-Stage models. These values are taken from

Parameter	Value
Optimizer	SGD
Learning Rate	0.01
Momentum	0.9
Batch Size	8
Seed	42
Epochs	20

Table 7: Hyperparameters used for the training of Two-Stage and Decoupled Two-Stage models.

previous work [5, 7, 8, 13, 15]. We trained the models for 20 epochs using early stopping (grace period=3). For each model, we evaluate the best epoch on the validation set (metric used: F1@K).

## References

- [1] Drew A. Hudson and Christopher D. Manning. GQA: A New Dataset for Real-World Visual Reasoning and Compositional Question Answering, May 2019.
- [2] Tianlei Jin, Fangtai Guo, Qiwei Meng, Shiqiang Zhu, Xiangming Xi, Wen Wang, Zonghao Mu, and Wei Song. Fast Contextual Scene Graph Generation With Unbiased Context Augmentation. pages 6302–6311, 2023.
- [3] Ranjay Krishna, Yuke Zhu, Oliver Groth, Justin Johnson, Kenji Hata, Joshua Kravitz, Stephanie Chen, Yannis Kalantidis, Li-Jia Li, David A. Shamma, Michael S. Bernstein, and Li Fei-Fei. Visual Genome: Connecting Language and Vision Using Crowdsourced Dense Image Annotations. *International Journal of Computer Vision*, 123(1):32–73, May 2017. ISSN 1573-1405. doi: 10.1007/s11263-016-0981-7.
- [4] Alina Kuznetsova, Hassan Rom, Neil Alldrin, Jasper Uijlings, Ivan Krasin, Jordi Pont-Tuset, Shahab Kamali, Stefan Popov, Matteo Mallocci, Alexander Kolesnikov, et al. The open images dataset v4: Unified image classification, object detection, and visual relationship detection at scale. *International journal of computer vision*, 128(7):1956–1981, 2020.
- [5] Xin Lin, Changxing Ding, Jinquan Zeng, and Dacheng Tao. GPS-Net: Graph Property Sensing Network for Scene Graph Generation. In *2020 IEEE/CVF Conference on Computer Vision and Pattern Recognition (CVPR)*, pages 3743–3752, Seattle, WA, USA, June 2020. IEEE. ISBN 978-1-72817-168-5. doi: 10.1109/CVPR42600.2020.00380.
- [6] Maëlic Neau, Paulo Santos, Anne-Gwenn Bosser, and Cédric Buche. In defense of scene graph generation for human-robot open-ended interaction in service robotics. In *Robot World Cup*, pages 299–310. Springer, 2023.
- [7] Kaihua Tang, Hanwang Zhang, Baoyuan Wu, Wenhan Luo, and Wei Liu. Learning to Compose Dynamic Tree Structures for Visual Contexts. In *2019 IEEE/CVF Conference on Computer Vision and Pattern Recognition (CVPR)*, pages 6612–6621, Long Beach,

- CA, USA, June 2019. IEEE. ISBN 978-1-72813-293-8. doi: 10.1109/CVPR.2019.00678.
- [8] Kaihua Tang, Yulei Niu, Jianqiang Huang, Jiaxin Shi, and Hanwang Zhang. Unbiased Scene Graph Generation From Biased Training. In *2020 IEEE/CVF Conference on Computer Vision and Pattern Recognition (CVPR)*, pages 3713–3722, Seattle, WA, USA, June 2020. IEEE. ISBN 978-1-72817-168-5. doi: 10.1109/CVPR42600.2020.00377.
- [9] Ao Wang, Hui Chen, Lihao Liu, Kai Chen, Zijia Lin, Jungong Han, and Guiguang Ding. Yolov10: Real-time end-to-end object detection. *arXiv preprint arXiv:2405.14458*, 2024.
- [10] Chien-Yao Wang, I-Hau Yeh, and Hong-Yuan Mark Liao. Yolov9: Learning what you want to learn using programmable gradient information. *arXiv preprint arXiv:2402.13616*, 2024.
- [11] Danfei Xu, Yuke Zhu, Christopher B. Choy, and Li Fei-Fei. Scene Graph Generation by Iterative Message Passing. In *Proceedings of the IEEE Conference on Computer Vision and Pattern Recognition*, pages 5410–5419, 2017.
- [12] Jingkang Yang, Yi Zhe Ang, Zujin Guo, Kaiyang Zhou, Wayne Zhang, and Ziwei Liu. Panoptic Scene Graph Generation. In Shai Avidan, Gabriel Brostow, Moustapha Cissé, Giovanni Maria Farinella, and Tal Hassner, editors, *Computer Vision – ECCV 2022*, Lecture Notes in Computer Science, pages 178–196, Cham, 2022. Springer Nature Switzerland. ISBN 978-3-031-19812-0. doi: 10.1007/978-3-031-19812-0\_11.
- [13] Rowan Zellers, Mark Yatskar, Sam Thomson, and Yejin Choi. Neural Motifs: Scene Graph Parsing with Global Context. In *2018 IEEE/CVF Conference on Computer Vision and Pattern Recognition*, pages 5831–5840, Salt Lake City, UT, June 2018. IEEE. ISBN 978-1-5386-6420-9. doi: 10.1109/CVPR.2018.00611.
- [14] Ji Zhang, Yannis Kalantidis, Marcus Rohrbach, Manohar Paluri, Ahmed Elgammal, and Mohamed Elhoseiny. Large-Scale Visual Relationship Understanding, August 2019. arXiv:1804.10660 [cs].
- [15] Chaofan Zheng, Xinyu Lyu, Lianli Gao, Bo Dai, and Jingkuan Song. Prototype-based embedding network for scene graph generation. In *Proceedings of the IEEE/CVF Conference on Computer Vision and Pattern Recognition*, pages 22783–22792, 2023.